

ENERGY SPECTRA AND COMPOSITION OF PRIMARY COSMIC RAYS

DIETRICH MÜLLER, SIMON P. SWORDY, PETER MEYER, JACQUES L'HEUREUX,¹ & JOHN M. GRUNSFELD²

Enrico Fermi Institute and Department of Physics, University of Chicago, 933 East 56th Street, Chicago, IL 60637

Received 1990 August 16; accepted 1990 December 3

ABSTRACT

We describe new results on the energy spectra and relative abundances of primary cosmic ray nuclei from carbon to iron. The measurement was performed on the Spacelab-2 mission of the Space Shuttle *Challenger* in 1985, and extends to energies beyond 1 TeV per amu. The data indicate that the cosmic ray flux arriving near Earth becomes enriched with heavier nuclei, most notably iron, as energy increases. Extrapolating to the source, with a simple leaky box model of galactic propagation with rigidity-dependent containment time, we obtain relative abundances of the elements that are quite similar to those reported at lower energy. In particular, the depletion of elements with high first ionization potential relative to the local galactic abundances, seems to persist in the cosmic ray source well up to TeV energies. A single power-law energy spectrum $\sim E^{-2.1}$ provides a good description of the observed spectra of most elemental species.

Subject headings: cosmic rays: abundances — cosmic rays: general

1. INTRODUCTION

The nature of the sources and of the acceleration mechanisms of galactic cosmic rays has remained an elusive question in astrophysics for many years. It now seems likely that first-order Fermi acceleration near interstellar shock fronts can account for the observed cosmic ray flux up to energies around 10^{15} eV (for a review, see Axford 1981 and Völk 1987). The energy requirements are met if the shocks are powered by supernova explosions and if a significant fraction of the supernova energy is transferred to the cosmic rays. The mechanism leads naturally to power-law spectra in rigidity, proportional to $R^{-(2+\delta)}$ at the source, with R the particle rigidity and the parameter δ being related to the strength of the shock. The Galaxy has been pervaded by a steady cosmic ray flux for at least 10^9 yr, a time period that much exceeds the average containment time of $\sim 10^7$ yr or less of individual cosmic ray particles. Thus, cosmic ray accelerators seem to be ever-present, and the contemporaneous flux may well have its origin in a variety of acceleration sites. Experimental information on these phenomena comes from the analysis of the arriving cosmic ray flux. Key questions of present observations are the following:

1. Does the composition of the cosmic rays at the acceleration sites represent that of the interstellar medium or are there contributions from specific stellar objects, or from freshly synthesized supernova ejecta?
2. Are the energy spectra for all species characterized by smooth power laws, or are there variations due to contributions from different sources?

In order to obtain the primary spectra at the acceleration sites from the data measured near Earth, a propagation calculation is required that takes into account interactions, energy losses and escape from the galaxy, and the generation of secondary particles during interstellar propagation, as well as the local effects due to solar modulation. At low energies ($\lesssim 10$ GeV per amu) where the most precise measurements exist, such

calculations are fairly involved and depend on a number of parameters that are not well-known, such as nuclear interaction cross sections and their variations with energy, and the details of solar modulation. Nevertheless, the data indicate that cosmic rays are *accelerated* to power-law spectra in rigidity but that the *observed* spectra above a few GeV per amu are considerably steeper, due to rigidity-dependent escape of particles from the galaxy. There is **no** strong indication for a change of the source composition with energy. However, the energy region over which this could be tested with some precision and without uncertainty due to solar modulation is quite small, covering about one decade in energy.

The extrapolation of cosmic ray measurements to the sources becomes much more straightforward at higher energies: effects due to solar modulation are then insignificant, ionization energy losses during propagation may be neglected, and the nuclear interaction cross sections can be assumed to be independent of energy. One therefore wishes to extend the measurements to higher energies, but due to the steepness of the cosmic ray spectrum this requires the availability of large detectors and long exposure times. In addition, the energy measurement of highly relativistic nuclei provides a serious challenge to the experimenter.

In this paper, we present and discuss results on the nuclear composition of cosmic rays obtained with a detector that we have developed in order to reach energies well beyond the TeV per amu region. With sufficient exposure time, our instrument is capable of approaching the region of the spectral break that has been observed above 10^{15} eV on the basis of air shower data (for a compilation of recent data, see Hara et al. 1983). In the region of overlap, our detector can provide a test and calibration of the air shower technique which is the only means available to extend cosmic ray measurements to the very highest particle energies known.

The instrument employs the first transition radiation detector designed to measure the energy of cosmic ray nuclei. It was developed for flights on the Space Shuttle but can also be adapted to missions of longer duration. A first flight onboard the Space Shuttle *Challenger* took place in 1985. Initial results from this exposure were reported previously (contributions of the International Cosmic Ray Conferences in Moscow, 1987,

¹ Present address: Bartol Research Institute, University of Delaware, Newark, DE 19716.

² Present address: California Institute of Technology, 220-47, Pasadena, CA 91106.

and Adelaide, 1990; Grunsfeld et al. 1988; Swordy et al. 1990a). In the following, we concentrate on the measurement of the energy spectra of the "primary" cosmic ray nuclei, i.e., those that are accelerated at the source (in contrast to secondary nuclei that are generated by spallation in interstellar space). Our instrument was not designed to detect the light nuclei H and He, thus this report covers the heavier species, from carbon to iron. We shall deduce the spectra and the composition of these nuclei at the acceleration site, and we shall discuss constraints on the source mechanism on the basis of our data.

2. OBSERVATIONAL DETAILS

2.1. Instrument Description

Figure 1 shows a schematic cross section of the instrument (usually referred to as Cosmic Ray Nuclei Detector or CRN) that was developed for this measurement. A detailed description of the design and performance of this instrument is given elsewhere (L'Heureux et al. 1990). In the present report, we shall summarize just briefly the relevant features: the instrument employs plastic scintillators (T1, T2), gas Čerenkov counters (C1, C2) and a transition radiation detector (TRD). This combination permits the measurement of the following quantities for each cosmic ray nucleus traversing the detector:

1. atomic number, i.e., the nuclear charge Z ,
2. energy E , over the range 40 GeV per amu to several TeV per amu,
3. trajectory and direction of incidence of the particle,

The determination of energy and charge utilizes the characteristic dependence on both Z and E of the various counter signals. These dependences have been determined in extensive calibrations at accelerators before the flight, and through consistency checks using the flight data themselves.

The scintillators are the major charge measuring devices, utilizing the Z^2 dependence of the ionization loss. Their signals are nearly independent of energy over the range of concern here. The scintillators also provide the coincidence trigger and the signals for the time of flight measurement.

The two gas Čerenkov counters are filled with a N_2/CO_2 mixture at 1 atm. For fixed energy per amu, their signals are proportional to Z^2 . Above the Čerenkov threshold at ~ 40 GeV per amu, the signals increase rapidly with E until saturation is reached at about 150 GeV per amu. They therefore provide an energy measurement between 40 and 150 GeV per amu.

At higher energy, the transition radiation detector performs the energy measurement. It consists of six pairs of plastic fiber radiators and multiwire proportional chambers (MWPC), chosen such that the detection threshold for transition radiation is reached at about 500 GeV per amu. For energies below 500 GeV per amu, the MWPCs measure the ionization loss of the particle whose approximately logarithmic rise with energy is used for a coarse energy assignment. Above 500 GeV per amu the yield of transition radiation X-rays rises rapidly with energy up to at least several TeV per amu and provides an excellent energy measurement. Both the ionization loss and the transition radiation signals scale with Z^2 . We expect the TRD

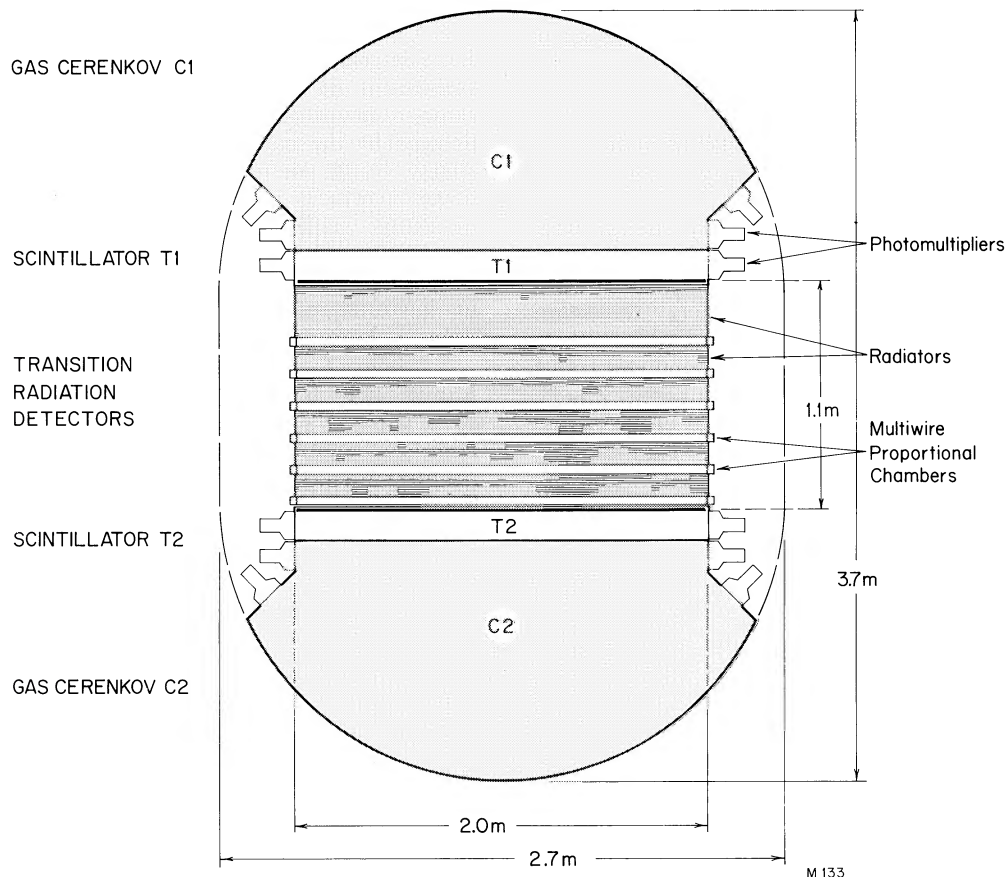


FIG. 1.—Schematic cross section of the CRN detector

to reach saturation around 5–10 TeV per amu. However, due to the limited exposure time we did not obtain cosmic ray data near the TRD saturation region. In addition to the energy measurement, the MWPCs also provide position information to reconstruct the trajectory of a traversing particle.

This design of our instrument was led by the following criteria:

1. *Weight and exposure factor.* To maximize the exposure factor, we constructed a detector whose size was only restricted by the dimensions of the Space Shuttle cargo area. This mandated energy measuring techniques that can be implemented for large areas without making the instrument excessively massive.

2. *Redundant measurements.* All measurements are performed with a high degree of redundancy. We request consistent signals for the *two* scintillators, and for the *two* Čerenkov counters. Further, each scintillator and each Čerenkov counter is read out through several independent sets (two or three, respectively) of photomultipliers, of which we request consistency for valid events. The TRD performs *six* independent measurements which must be consistent with each other (for details, see L'Heureux et al. 1990). We also cross-correlate the signals of the energy measuring devices: for a valid event in the Čerenkov regime (40–150 GeV per amu), the TRD must show no indication of transition radiation X-rays, and for a valid TR event (above 500 GeV per amu), the Čerenkov signal must be in saturation. This redundancy is essential for an unambiguous identification of the small flux of high-energy particles in the presence of a large background of low-energy cosmic rays.

2.2. Performance and Flight

In summary, the performance of the CRN instrument is characterized as follows:

1. Charge Resolution (rms).

$$\delta Z = \begin{cases} 0.2 \text{ charge units} & \text{for oxygen } (Z = 8) \\ 0.35 \text{ charge units} & \text{for iron } (Z = 26). \end{cases}$$

The charge resolution does not significantly change with energy.

2. *Energy Resolution.* Due to the nonlinear response of both the Čerenkov counters and the TRD, the energy resolution changes with energy. Also, it improves with increasing charge Z . Typical rms values of $\delta E/E$ at 100 GeV per amu and 1 TeV per amu, respectively, are 35% and 11% for oxygen ($Z = 8$), and 13% and 8% for iron ($Z = 26$). The widths of the energy intervals into which we will group our results (Table 1 and Fig. 3) are chosen to reflect both the energy resolution and the limited counting statistics of the data.

3. *Trajectory Resolution.* The trajectory of each cosmic ray particle through the instrument is measured with a spatial resolution of 1.4 cm rms, and the direction of incidence is determined with an accuracy of about 1° .

The CRN instrument was flown in 1985 July/August in the Spacelab-2 mission of the Space Shuttle *Challenger*. While the total flight duration was about 8 days, the net observation time at full aperture amounted to 78 hr. This reduction in exposure was caused by many conflicting requirements on the attitude of the spacecraft due to other instruments onboard, and by parts of the orbit in high-radiation environments (the tips of the radiation belts, and the South Atlantic Anomaly).

2.3. Data Analysis

The data analysis procedures have been previously described (Swordy et al. 1990a). In brief, the analysis proceeds along the following steps.

1. *Trajectory Reconstruction and Pulse Height Normalizations.* For each accepted event, the trajectory through the detector is determined, and the pulse heights are corrected for position and angle of incidence, taking the spatial nonuniformities of the detector response into account. As the path length of the particle through the Čerenkov counter varies significantly from event to event, the Čerenkov signals are normalized for path length variations. This normalization is done after a background of light emission from the high-reflectance white paint coating of the counters is subtracted (for details, see L'Heureux et al. 1990). The TRD signal scales *approximately* as $1/\cos \theta$, where θ is the angle between the particle trajectory and the axis of the instrument (see Swordy et al. 1990b).

2. *Charge and Energy Determination.* Charge Z and energy E are determined for each nucleus traversing the instrument by comparing the set of measured pulse heights x_i with known response functions $p_i(x_i, Z, E)$ which describe for each counter (labeled by the index i) the probability that a particle with charge Z and energy E produces a pulse height x_i . For the lower charges ($Z \leq 8$) we use a maximum likelihood technique to ascribe values Z and E (see Swordy et al. 1990a). For charges $Z > 8$, the functions p_i become nearly Gaussian, and a simple least χ^2 procedure is sufficient to determine Z and E . As an illustration of the charge resolution of this detector, Figure 2 shows charge histograms selected for nuclei at high energies.

3. *Monte Carlo Model.* We have developed a detailed Monte Carlo model of the instrument response to an energy spectrum of relativistic nuclei close to that expected for cosmic rays. The simulation determines a realistic signal for all counters traversed by each nucleus, including the details of fluctuations as determined from the flight data. These Monte

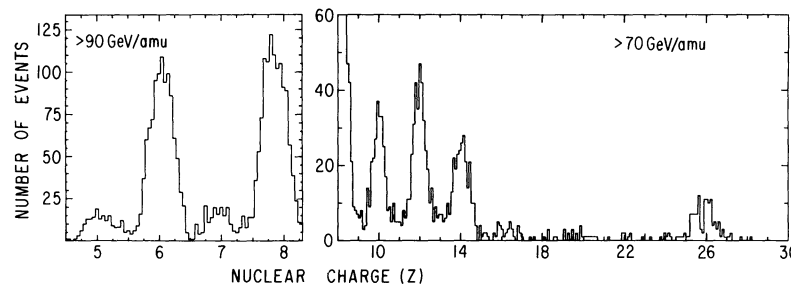


FIG. 2.—Charge histograms of cosmic ray nuclei. Events displayed were chosen to correspond to high-energy particles on the basis of the signals in the gas Čerenkov counters.

Carlo events are then subjected to the same analysis routines used for the flight data to obtain the efficiency of the various cuts applied to the data. The simulated events are also used to determine the corrections due to the limited and varying energy resolution of the detector that are necessary to derive the energy spectrum of cosmic rays from the energy ordered set of recorded events (for details, see Swordy et al. 1990a).

4. *Absolute Flux Normalization.* The final step in the data analysis is to determine the absolute flux of cosmic rays entering the instrument. This requires an assessment of the effective exposure factor of the instrument. We have developed a second Monte Carlo model which is used to calculate this factor; the Spacelab-2 flight is divided into a sequence of small intervals (~ 1 minute) within which the spacecraft location and detector counting rates have negligible changes. In each of these intervals an isotropic flux of particles is allowed to traverse the detector and each nucleus is followed through the detector, taking all materials due to counters, structural members, etc., into account. The probability that the nucleus undergoes a spallation reaction is calculated, using the spallation cross sections of Westfall et al. (1979) which are independent of energy (see § 4 for further details). Nuclei are also rejected if they appear to arrive from a direction below a "horizon" at 90° to the zenith, in order to remove particles which may have interacted with the Earth's atmosphere. The effective instrument dead times and the geometric acceptance factors are then calculated for each time period, and summed to provide the effective exposure factor for each nuclear species for the entire flight. We have previously given a summary of the average numerical values of the various factors which contribute to the overall exposure factor (Swordy et al. 1990a) but we were left with a small systematic uncertainty that led us to present our data with an arbitrary overall normalization: we chose the differential flux of oxygen nuclei at 73 GeV per amu to agree with the average of previous oxygen data at that energy [$= 2.02 \times 10^{-4} (\text{m}^2 \text{sr s GeV per amu})^{-1}$].

Further detailed analysis of the cuts applied to the data has considerably reduced this remaining uncertainty. This permits us now to present absolute fluxes. For instance, our result for the oxygen flux at 73 GeV per amu is $(1.88 \pm 0.18) \times 10^{-4} (\text{m}^2 \text{sr s GeV per amu})^{-1}$. Our previous normalization lies within the uncertainty limit of the present result.

3. RESULTS

Because of limitations in the dynamic range of the detector, and due to the inherent magnitude of fluctuations in the transition radiation and Čerenkov signals, the CRN instrument was not designed to provide observations of protons and alpha particles. Thus, the major *primary* nuclei observed are carbon, oxygen, neon, magnesium, silicon, and iron. In Table 1 we show the particle fluxes of these elements. Note that the data for "iron" include the neighboring elements manganese and cobalt. The differential energy spectra are shown in Figure 3 and are compared with results of previous measurements, mostly obtained with balloon-borne instruments. The error limits given for our results in the table and in Figure 3 (and in the following figures) are statistical and are representative for Poisson distributions: the upper and lower limits, respectively, are 84% confidence limits as defined by Regener (1951) and Gehrels (1986). In comparing our data with others, one must take into account that other authors frequently use the Gaussian limit for n counts, $n \pm \sqrt{n}$, even if n is small.³ We empha-

³ We are grateful to Mark Wiedenbeck and Alan Watson for helpful discussions on the statistics of small numbers.

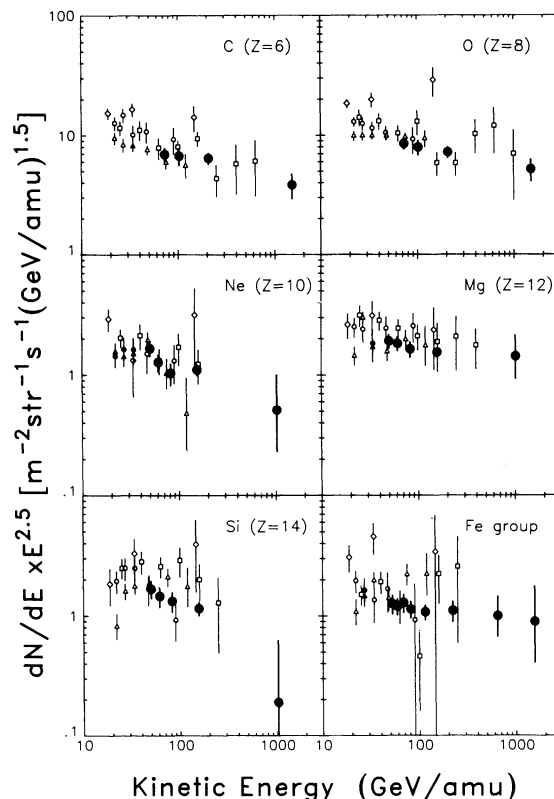


FIG. 3.—Differential energy spectra for the cosmic ray nuclei C, O, Ne, Mg, Si, and Fe. Note that the fluxes are multiplied with $E^{2.5}$. The solid data points refer to the present results, while the open symbols come from previous balloon work; circles: Caldwell (1977); squares: Simon et al. (1980); triangles: Juliussen (1974); diamonds: Orth et al. (1978).

size that the particle fluxes are measured *near Earth*. The extrapolation to obtain the spectra near the sources will be discussed below.

We had previously reported preliminary results on the spectra of the same elements (Grunsfeld et al. 1988). Our present result is based on a larger sample of data, and is obtained with more rigorous data analysis techniques. The present data agree well, within the quoted error bars, with our earlier result. However, as mentioned above, we have now quantitatively determined all instrumental efficiency corrections. *Our present data represent the absolute particle fluxes, without any normalization to previous measurements.* We estimate the overall normalization to be uncertain to not more than $\pm 10\%$. A qualitative inspection of the data shown in Figure 3 confirms our earlier conclusion that the spectrum of the iron group nuclei is flatter than that of all other species, and that the spectrum of silicon and perhaps that of neon is quite steep. We shall discuss these features in more detail in the following section.

Figure 4 shows the abundances of carbon and of the iron group relative to oxygen, covering a large range of energies. This figure includes data obtained with our instrument at energies of a few GeV per amu, where we have used the rigidity cutoff properties of the Earth's magnetic field for an energy determination. This procedure has been described previously (Swordy et al. 1990a). The solid lines are the results of a propagation calculation described below. They indicate that our data are consistent with a slight decrease of the abundance of

TABLE 1
DIFFERENTIAL FLUX VERSUS ENERGY FOR PRIMARY NUCLEI

Element	γ Range	Number of Events	Median Kinetic Energy ^b (GeV)	Flux $\times 10^6$ (m ² sr s GeV per amu) ⁻¹
C ^a	70-90	60	72.6	154 \pm 20
Z = 6	90-150	37	102.6	62.6 \pm 37
	150-800	90	206.8	10.4 \pm 1.1
	1100-10000	18	1503	0.0435 \pm .01
O ^a	70-90	109	72.6	188 \pm 18
Z = 8	90-150	55	102.6	73.8 \pm 10
	150-800	93	206.8	11.6 \pm 1.2
	1100-10000	23	1503	0.059 \pm .012
Ne	50-60	56	50.0	93.0 \pm 12.6
Z = 10	60-75	38	61.3	43.3 \pm 7.0
	75-115	23	82.7	16.5 \pm 3.4
	115-750	96	155.1	3.67 \pm 3.7
	750-10000	3	1028	0.0150 ^{+0.0142} _{-0.0081}
Mg	50-60	63	50.0	107.0 \pm 13.6
Z = 12	60-75	59	61.3	61.5 \pm 7.9
	75-115	48	82.7	26.1 \pm 3.7
	115-750	136	155.1	4.86 \pm .41
	750-10000	8	1028	0.0419 ^{+0.029} _{-0.014}
Si	50-60	37	50.0	94.6 \pm 15.4
Z = 14	60-75	28	61.3	49.4 \pm 9.3
	75-115	29	82.7	21.3 \pm 3.9
	115-750	65	157	3.72 \pm .47
	750-10000	1	1028	0.0056 ^{+0.0126} _{-0.0046}
Fe ^c	55-60	28	52.6	62.3 \pm 11.1
25 < Z < 27	60-70	37	59.2	44.3 \pm 6.7
	70-80	32	68.6	32.9 \pm 5.7
	80-100	31	81.6	18.8 \pm 3.0
	100-175	38	115.4	7.5 \pm 1.0
	175-440	27	222.0	1.5 \pm 0.28
	440-1100	9	649.0	0.0924 ^{+0.0412} _{-0.0302}
	1100-10000	3	1563	0.00923 ^{+0.00877} _{-0.00501}

^a The highest energy data points ($\gamma > 1100$) for carbon and oxygen were determined with less restrictions on the aperture of the detector than the data at lower energy ($\gamma < 800$).

^b The computation of the median kinetic energy for an energy interval requires knowledge of the spectral slope which is obtained by iteration for each spectrum.

^c Due to the higher Z^2 , the energy resolution for iron is significantly better than that for the other elements; therefore, it is meaningful to divide the data into finer increments in energy.

carbon relative to oxygen, and with a small increase of the relative iron abundance.

Figure 5 presents some results on the abundances relative to iron of the nuclei of sulfur ($Z = 16$), argon ($Z = 18$), and calcium ($Z = 20$). Again, our low-energy result comes from the geomagnetic cutoff analysis. The fluxes of these nuclei are quite low, and within the exposure time available, we did not obtain statistically significant data beyond ~ 100 GeV per amu. At low energy, these nuclei are known to have significant secondary contributions due to spallation of heavier nuclei (mostly iron) in the interstellar gas. As the propagation path length decreases with energy (Swordy et al. 1990a), the relative abundances of these nuclei are expected to decrease as well, as confirmed by the data. The slight decrease of the carbon abundance shown in Figure 4 can be explained in the same way, i.e., by the decrease of the small fraction of carbon that is produced by spallation. Figure 5 shows that the relative abundance of S, A, and Ca measured in our experiment at 100 GeV per amu is close to the source abundances deduced by Hinshaw & Wiedenbeck (1983) for sulfur, and by Binns et al. (1988) for argon and calcium.

It is instructive to express our data as spectra in total energy per nucleus, and to compare our results with the "all-particle spectrum" (Hara et al. 1983), that uses air shower data to

represent the overall cosmic ray flux up to the highest observed energies. This is shown for four elements in Figure 6. Clearly, our data indicate that the relative contribution of iron nuclei to the cosmic ray flux increases as we approach energies around 10^{14} eV. It is obviously of great interest to determine how the spectra of the individual components continue towards still higher energies, approaching the "knee" above 10^{15} eV. The present data, if extrapolated by single power laws for each component (with spectral indices varying from 2.55 to 2.80) would indicate a continuous enhancement of iron in the total cosmic ray flux. However, simple propagation models lead us to expect a gradual steepening of the the iron spectrum at higher energies. This will be discussed in the following section.

4. ABUNDANCES AT THE SOURCE AND NEAR EARTH

To derive the elemental abundances and energy spectra at the cosmic ray source from the data measured near Earth, a propagation calculation is required, the details of which depend on the assumed model of cosmic ray confinement in the galaxy. The simplest such model is known as the "leaky box model" and is used in our calculation in the following form:

$$Q_i(E) = \frac{N_i(E)}{\tau(E)} + N_i \sigma_i n c - \sum_{j>i} N_j \sigma_j n c. \quad (1)$$

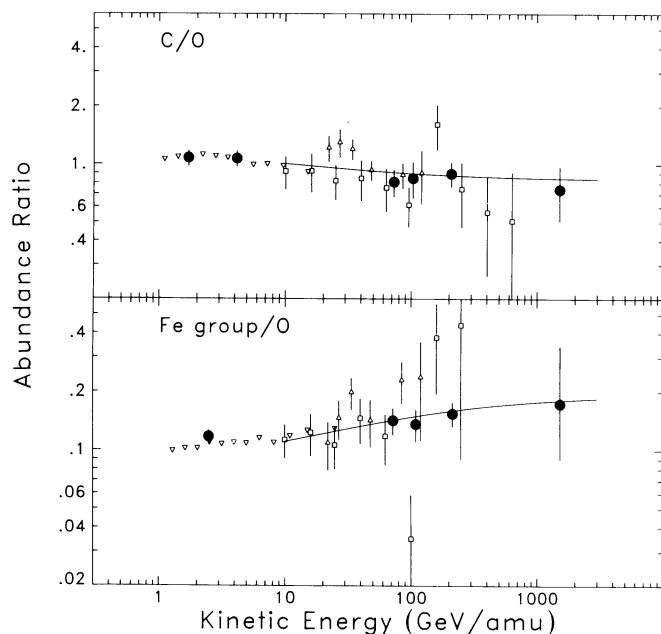


FIG. 4.—Abundances of carbon ($Z = 6$) and of the iron group ($25 \leq Z \leq 27$) relative to oxygen. Solid points: this work; other symbols as in Fig. 3; in addition, inverted triangles: Engelmann et al. (1985). The solid line describes the result of a propagation calculation (see text).

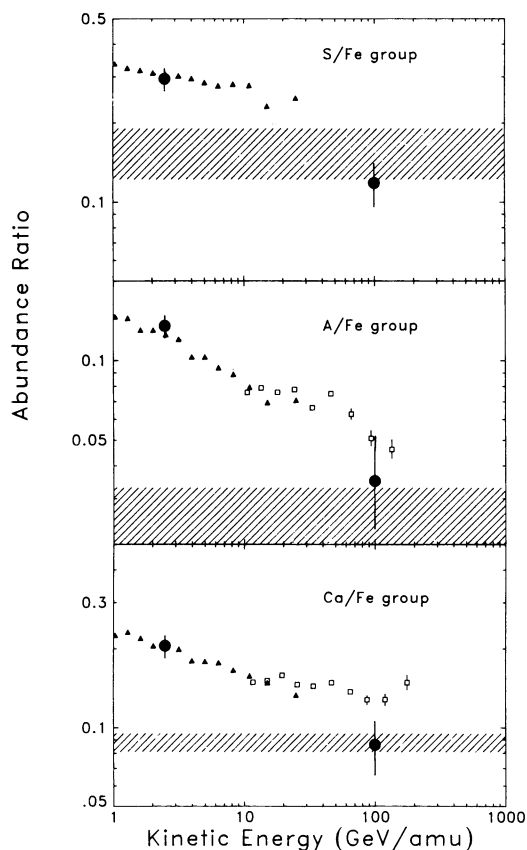


FIG. 5.—Abundances of sulfur ($Z = 16$), argon ($Z = 18$) and calcium ($Z = 20$), relative to iron ($25 \leq Z \leq 27$). Solid data points: this work; solid triangles: Engelmann et al. (1983); open squares: Binns et al. (1988). The shaded regions indicate the expected ranges of these abundance ratios at the source, according to previous work (see text).

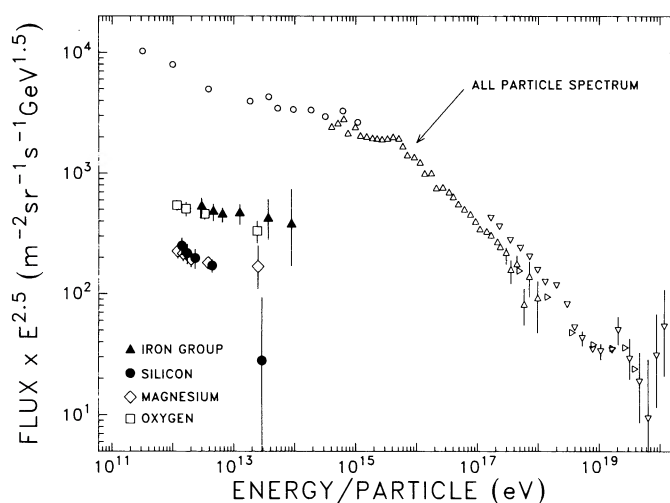


FIG. 6.—Energy spectra of several elements, plotted versus total energy per particle, and compared with the “all-particle spectrum.”

Here, N_i denotes the measured cosmic ray density of species i in an energy interval around E . We assume dynamic equilibrium between production and loss. Primary cosmic rays of species i are produced at a source rate $Q_i(E)$, and they escape from the galaxy after an average containment time $\tau(E)$, or they may be lost due to spallation with the interstellar gas (n is the number density of interstellar gas, σ_i denotes the spallation cross section, and c is the speed of the particles, virtually equal to the speed of light for our energy region). Species i can also be produced by spallation of heavier nuclei, $\sigma_{ji}(E)$ denotes the cross section for producing species i from species j .

Equation (1) is the simplified version of a more general expression: we replace the diffusion term describing the propagation through the galactic medium, by a containment time $\tau(E)$. Further, we neglect energy losses—a valid assumption for highly relativistic nuclei—but we also assume that there are no energy gains (which would be significant in “continuous acceleration” models). For the energy region of concern, we are justified to ignore solar modulation. Also, the spallation cross sections are assumed to be energy-independent at these energies. For our calculation, we use the cross sections in the parameterization of Tsao & Silberberg (1979). We should note that further experimental tests on the energy dependence of spallation cross sections would be desirable. For instance, recent measurements at Brookhaven and CERN (Price et al. 1988) have shown an increase in the cross section due to electromagnetic dissociation (EMD) at high energies. However, this effect is noticeable only for interactions with heavy targets and should not affect our propagation model (where hydrogen is the predominant target in the interstellar medium). Spallation reactions in the detector itself (discussed in § 2.3) do involve heavier targets, but again, the EMD effect is too small to be of concern. For instance, Price et al. (1988) report a $\sim 10\%$ increase in the cross section of sulfur ($Z = 16$) on aluminum ($Z = 13$) at 200 GeV per amu. As the aluminum content of our detector is about 0.01 interaction lengths, the EMD contribution would affect our measured fluxes at the 0.1% level, which is insignificant compared to other uncertainties.

The containment time τ is proportional to the propagation pathlength λ ($\lambda = \rho c \tau$, with ρ the average mass density of interstellar gas). We use the dependence of λ on the particle rigidity

TABLE 2
GALACTIC COSMIC RAY SOURCE/LOCAL GALACTIC
ABUNDANCE RATIO^a

Element	Ratio at 100 GeV per amu	Ratio at 1 TeV per amu
C	0.27 ± 0.05	0.20 ± 0.05
N	0.11 ± 0.03	≤ 0.16
O	0.20 ± 0.03	0.17 ± 0.04
Ne	0.16 ± 0.03	$0.10^{+0.095}_{-0.054}$
Mg	0.90 ± 0.13	$1.00^{+0.48}_{-0.35}$
Si	0.82 ± 0.15	$0.11^{+0.330}_{-0.090}$
S	0.18 ± 0.03	
Ar	0.19 ± 0.07	
Ca	0.71 ± 0.16	
Fe group	1.00 ± 0.15	$1.00^{+0.44}_{-0.33}$

^a Normalized to iron.

R as derived from measurements of the relative abundances of secondary and primary cosmic rays (Swordy et al. 1990):

$$\lambda(R) = 6.9 \left(\frac{R}{20 \text{ GV}} \right)^{-0.6} \text{ g cm}^{-2} \text{ for } R > 20 \text{ GV} \quad (2)$$

With these assumptions, we derive from the measured values $N_i(E)$ the source abundances $Q_i(E)$ for two energies, at 100 GeV per amu and 1000 GeV per amu.

In order to investigate to which extent the elemental composition of the cosmic ray source resembles that of the contemporaneous interstellar medium, we compare the source abundances with the local galactic abundance distribution (Meyer 1985a). This is shown in Table 2 and in Figure 7. Following the practice of previous studies at lower energy, we plot the ratios of cosmic ray source abundances to local galactic element abundances against the first ionization potential (FIP), with a normalization at iron. The low-energy measurements had shown (see, e.g., Meyer 1985b, and Fig. 7; *upper panel*) that the cosmic ray abundances follow a pattern of depletion with increasing first ionization potential. It appears on the basis of our present result (Fig. 7; *middle and lower panels*), that this pattern is well-preserved for the cosmic ray sources up to TeV energies. With a few exceptions, the relative abundances of the elements agree well at low and high energies, indicating that the cosmic ray composition at the source does not change significantly with energy. However, we must point out the exceptions: silicon seems underabundant at high energy, and both the hydrogen and helium abundances of previous measurements do seem to show variations inconsistent with this simple picture.

Contrary to the apparent energy independence at the source, the composition of the cosmic ray flux near Earth does change with energy. This is most noticeable in the relatively flat spectrum of iron. However, this can be explained in the leaky box model as a consequence of the competition between losses due to spallation, with an energy independent spallation path length of 2.3 g cm^{-2} (for iron), and losses due to energy-dependent escape, with an escape path length that decreases from $\sim 7 \text{ g cm}^{-2}$ at low energy to $\sim 1 \text{ g cm}^{-2}$ at 1 TeV per amu. We illustrate this with a propagation calculation in which we assume that the energy spectra at the source are proportional to $E^{-2.1}$ for all species. We further take the abundances at the source to be the same as those derived for low energies by Hinshaw & Wiedenbeck (1983), with the exception of iron, where a value 15% higher than that given by Hinshaw

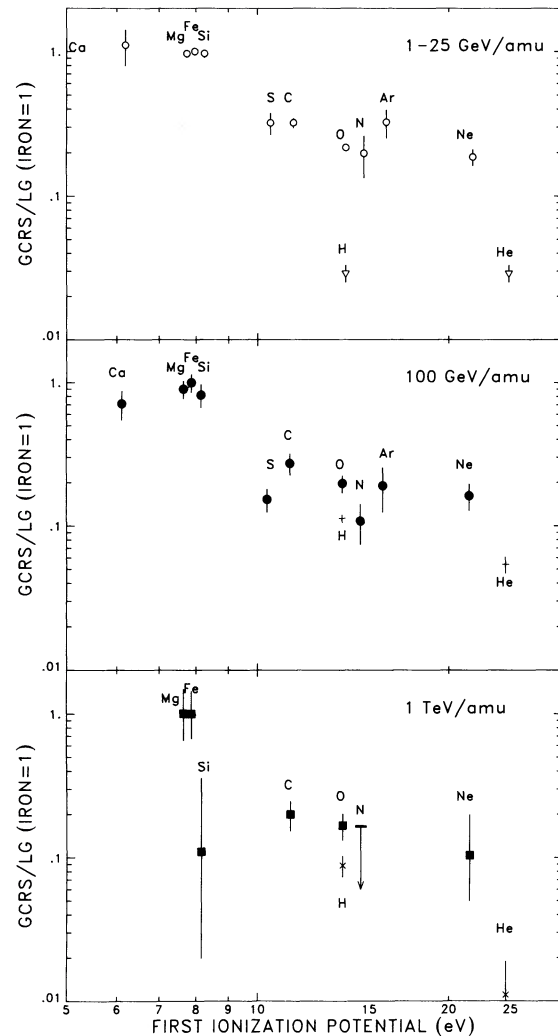


FIG. 7.—Abundances of the galactic cosmic ray nuclei at the source (GCRS), relative to the local abundance (LG), plotted against the values of the first ionization potentials of the elements. *Upper panel*: previous results at low energy (1–25 GeV per amu; data from Koch-Miramond 1983); *middle and lower panels*: high-energy results from the present work at 100 and 1000 GeV per amu, respectively. The figure also includes data on the hydrogen and helium abundances (*upper panel*: Smith et al. 1973; *middle and lower panels*: Ryan et al. 1972). All abundances are relative to iron.

& Wiedenbeck (1983) is chosen to give better agreement with our data. With an escape path length given by equation (2), we then compute the resulting spectra near Earth. These spectra are shown as solid lines in Figure 8 and the calculated ratios as lines in Figure 4. We emphasize that these results come from a propagation calculation with a priori assumptions as described, but are not meant to provide the best fit to our measurements. Nevertheless, the calculated spectra agree fairly well with the data, and, in particular, indicate a relatively flat iron spectrum. Some of our measurements, most noticeably the spectra of silicon and neon, are however not well described by the model.

The more energetic nuclei measured by this instrument have sufficient energy to produce sizeable air showers which can be observed by counter arrays at ground level. Therefore, these direct measurements of the elemental composition provide a calibration for attempts to determine the composition from air

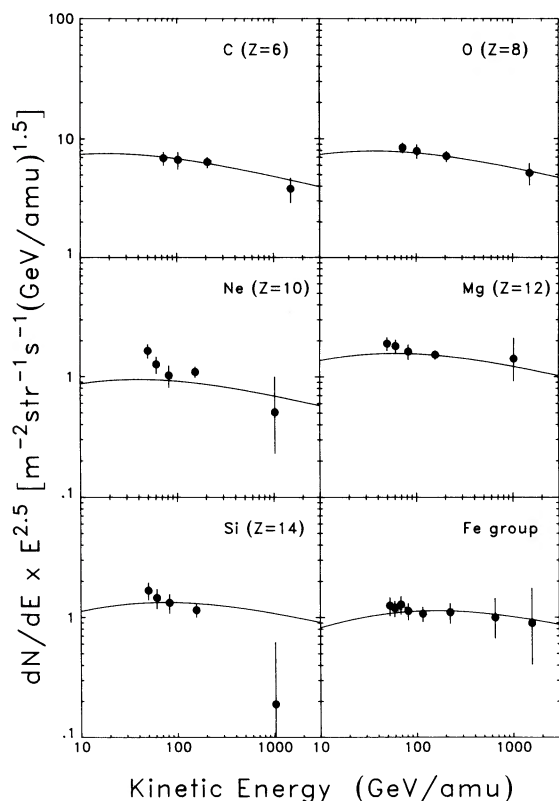


FIG. 8.—Measured energy spectra of the major primary nuclei (solid data points) compared with the result of a propagation calculation (curves; see text for details). The data points shown are the same as in Fig. 3.

shower data alone. In Figure 9 we show the fractional contributions of individual cosmic ray components to the total cosmic ray intensity (as given in Fig. 6) over the range 10^{12} to 10^{14} eV per particle. Also shown is the prediction of the leaky box model described above.

It can be seen that the Fe abundance fraction increases steadily from $\sim 5\%$ to 12% , the proportions of C and O, however, remain relatively constant. Figure 10 shows the overall contribution according to our model to the total cosmic ray intensity, cumulative for the species measured here. As data and model agree fairly well, we conclude that the contribution of heavy nuclei measured in our experiment to the overall flux may become as large as 35% in the 10^{13} – 10^{14} eV range. This is to be compared with a proton fraction of approximately 25% at 10^{14} eV (Burnett et al. 1990).

5. DISCUSSION AND CONCLUSIONS

The apparent depletion of cosmic ray source abundances with increasing first ionization potential (FIP) seems to be a pervasive feature that appears for galactic cosmic rays at all energies at which composition measurements have been possible. As measurements on the *HEAO-3* spacecraft have shown, the FIP parameter also orders the rare ultraheavy nuclei, beyond the iron group (Binns et al. 1989). Furthermore, the same pattern has been observed, at much lower energies, for solar energetic particles (Breneman & Stone 1985). Thus, this effect indicates a selection process based on atomic parameters that must occur before acceleration to relativistic energies takes place and that acts in the same fashion on a variety of

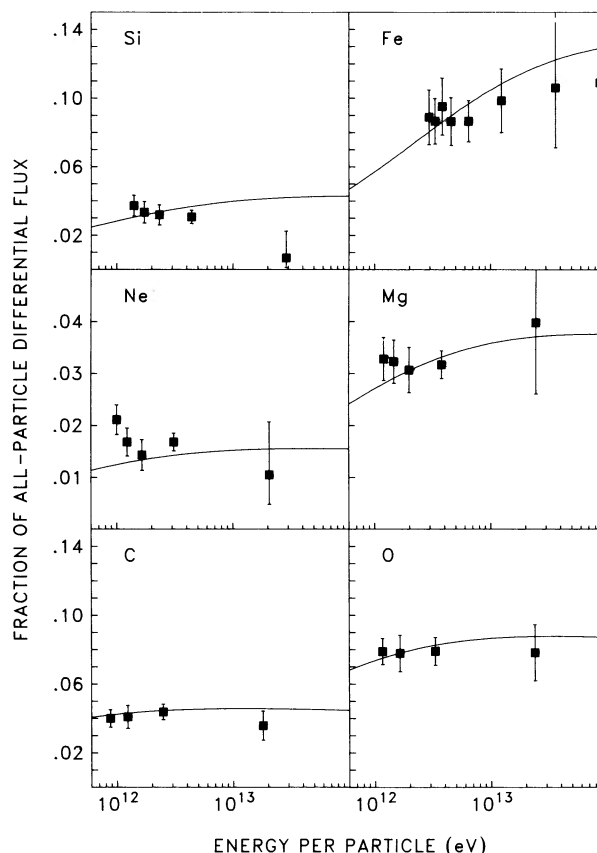


FIG. 9.—Fractions of the major cosmic ray nuclei, relative to the total flux given by the “all-particle” spectrum of Fig. 6. The data are plotted against the total energy per particle. The solid data points are measured values, and the curves are the results of a propagation calculation.

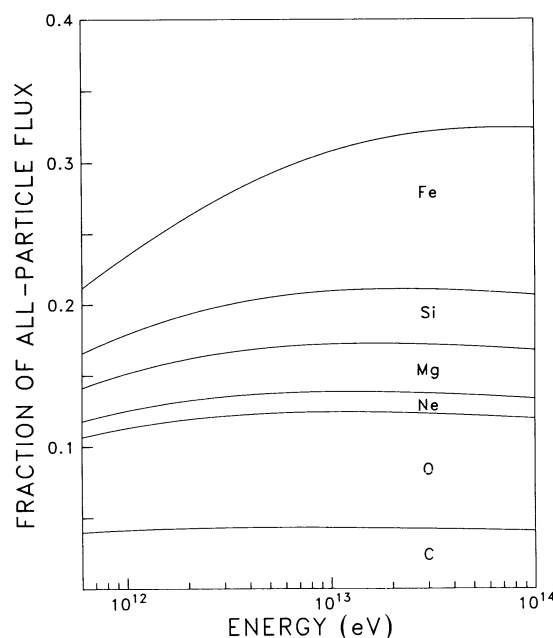


FIG. 10.—Fractions from propagation calculation as shown in Fig. 9, but plotted cumulatively versus the total energy per particle.

scales, from the solar chromosphere to galactic accelerators. The correlation with FIP may not be linear. Some authors, e.g., Silberberg & Tsao (1990), argue that the data indicate a sudden suppression of particles when the first ionization potential exceeds 10 eV. These authors then assume that a first-stage injection of cosmic ray particles takes place in stellar photospheres at temperatures around 10^4 K.

If we adopt this point of view, we are led to conclude that the bulk of the cosmic rays must be accelerated from material that originated in stellar eruptions or stellar winds and is enriched with ions formed in stellar photospheres. Some of this material might be from objects such as pre-supernova red giants, or from Wolf-Rayet stars. The latter have been proposed to account for the enhancement of the ^{22}Ne isotope (Meyer 1981). The stellar wind particles could then be subsequently boosted in energy in interstellar shocks (Völk & Biermann 1988). It remains uncertain, both within this model and on the basis of observational evidence, whether there is an appreciable contribution of fresh supernova-ejected material to the cosmic ray flux.

There are features in the data that are not consistent with any such picture. According to our results, the relative abundance of silicon drops by about a factor of 3 over the energy range 10–1000 GeV per amu. Additional data on silicon with improved counting statistics would be highly desirable. Further, the most abundant cosmic ray nuclei, protons and helium, do not fit well into the general FIP pattern, and the data published in the literature seem to exhibit changes of the relative abundances of these nuclei with energy. However, the suggestion by Engelmann et al. (1985) that different sources may be responsible for protons and alpha particles, and for heavier nuclei, respectively, needs to be supported with more accurate measurements of the high energy spectra of protons and helium than are presently available.

As the solid lines in Figure 8 show, our results are fairly consistent with the simplest model of a source with energy-independent composition and the source energy spectrum proportional to $E^{-2.1 \pm 0.1}$. This model would predict that all nuclear species, including iron, will attain the same spectral slope at sufficiently high energies. For a definitive test, data covering a larger energy interval are needed. The only experimental information presently available at higher energies comes from the JACEE group (Burnett et al. 1990). In Figure 11 we plot their results together with our data, combining several nuclear species to match with the more limited charge resolution of the JACEE detector. The figure illustrates that the uncertainty of the data in the 10^{14} eV per particle region is still too large as to permit a firm conclusion on the validity of the model. This situation would be greatly improved if our instrument were flown for an extended period of time, of the order of 1 yr. The limitation in energy coverage by CRN is entirely due to the limited exposure time. With a slight

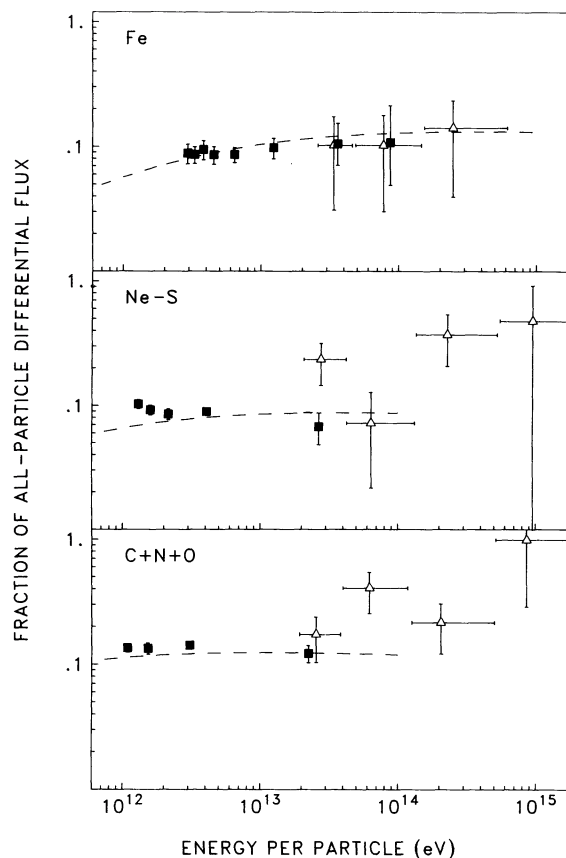


FIG. 11.—Abundances of three groups of elements ($25 \leq Z \leq 27$; $10 \leq Z \leq 16$; and $6 \leq Z \leq 8$) relative to the “all-particle” spectrum, vs. total energy per particle. Solid data points: present work, open triangles: data from Burnett et al. (1990); dashed lines: propagation calculation.

retuning of the transition radiation detector, the dynamic range of our technique extends to energies above 10 TeV per amu, one order of magnitude beyond our present result. We hope that such a long duration flight can be realized.

We gratefully acknowledge the contributions to the success of this investigation by the technical staff of our laboratory, in particular of L. Glennie, and D. E. Bonasera, E. Drag, W. Harvey, W. C. Johnson, and R. Ray, and of the Spacelab-2 team at NASA/Marshall Space Flight Center led by R. Lester. We are indebted to A. Borione M. Kamionkowski and L. Kawano for contributions to the data analysis effort. This work was supported by NASA under contract NAS 8-32828 and grants NAG W-1311, NGL-14-001-005 and NGL 14-001-258.

REFERENCES

- Axford, W. I. 1981, Proc. 17th Internat. Conf. on Cosmic Rays (Paris), 12, 155
 Binns, W. R., Fickle, R. K., Garrard, T. L., Israel, M. H., Klarman, J., Stone, E. C., & Waddington, C. J. 1981, ApJ, 247, L115
 Binns, W. R., et al. 1989, ApJ, 346, 997
 Binns, W. R., Garrard, T. L., Israel, M. H., Jones, M. D., Kamionkowski, M. P., Klarman, J., Stone, E. C., & Waddington, C. J. 1988, ApJ, 324, 1106
 Breneman, H. H., & Stone, E. C. 1985, ApJ, 299, L57
 Burnett, T. H., et al. (JACEE Collaboration) 1990, Proc. 21st Internat. Conf. on Cosmic Rays (Adelaide), 3, 101
 Caldwell, J. H. 1977, ApJ, 218, 269
 Engelmann, J. J., et al. 1983, Proc. 18th Internat. Conf. on Cosmic Rays (Bangalore), 2, 17
 Engelmann, J. J., Goret, P., Juliusson, E., Koch-Miramond, L., Lund, N., Masse, P., Rasmussen, I. L., & Soutoul, A. 1985, A&A, 148, 12
 Gehrels, N. 1986, ApJ, 303, 336
 Grunsfeld, J. M., L'Heureux, J., Meyer, P., Müller, D., & Swordy, S. P. 1988, ApJ, 327, L31
 Hara, T., et al. 1983, Proc. 17th Internat. Conf. on Cosmic Rays (Bangalore), 9, 198
 Hinshaw, G. F., & Wiedenbeck, M. E. 1983, Proc. 18th Internat. Conf. on Cosmic Rays (Bangalore), 9, 263
 Israel, M. H., et al. 1983, Proc. 18th Internat. Conf. on Cosmic Rays (Bangalore), 9, 305
 Juliusson, E. 1974, ApJ, 191, 331

- Koch-Miramond, L. 1981, Proc. 17th Internat. Conf. on Cosmic Rays (Paris), 12, 21
- L'Heureux, J., Grunsfeld, J. M., Meyer, P., Müller, D., & Swordy, S. P. 1990, Nucl. Instr. Meth., A295, 246.
- Meyer, J. P. 1981, Proc. 17th Internat. Conf. on Cosmic Rays (Paris), 2, 265
- . 1985a, ApJS, 57, 173
- . 1985b, Proc. 19th Internat. Conf. on Cosmic Rays (La Jolla), 9, 141
- Orth, C. D., Buffington, A., Smoot, G. F., & Mast, T. 1978, ApJ, 226, 1147
- Price, P. B., Guoxiao, R., & Williams, W. T. 1988, Phys. Rev. Letters, 61, 2193
- Regener, V. H. 1951, Phys. Rev., 84, 161
- Ryan, M. J., Ormes, J. F., & Balasubrahmanyam, V. K. 1972, Phys. Rev. Letters, 28, 985
- Silberberg, R., & Tsao, C. H. 1990, ApJ, 352, L49
- Simon, M., Spiegelhauer, H., Schmidt, W. K. H., Siohan, F., Ormes, J. F., Balasubrahmanyam, V. K., & Arens, J. F. 1980, ApJ, 239, 712
- Smith, L. H., Buffington, A., Smoot, G. F., Alvarez, L. W., & Wahlig, M. A. 1973, ApJ, 180, 987
- Swordy, S. P., Grunsfeld, J. M., L'Heureux, J., Meyer, P., Müller, D., & Tang, K. K. 1990b, Phys. Rev., D42, 3197
- Swordy, S. P., Müller, D., Meyer, P., L'Heureux, J., & Grunsfeld, J. M. 1990a, ApJ, 349, 625
- Tsao, C. H., & Silberberg, R. 1979, Proc. 16th Internat. Conf. on Cosmic Rays (Kyoto), 2, 202
- Völk, H. J. 1987, Proc. 20th Internat. Conf. on Cosmic Rays (Moscow), 7, 157
- Völk, H. J., & Biermann, P. L. 1988, ApJ, 333, L65
- Westfall, J. D., Wilson, L. W., Lindstrom, P. J., Crawford, H. C., Greiner, D. E., & Heckman, H. H. 1979, Phys. Rev., C19, 1309